

Statistics of AGN in Rich Clusters Revisited

M.J. Way^{1,2,3}, R.A. Flores and H. Quintana^{4,5}

Department of Physics and Astronomy, University of Missouri-St.Louis,
8001 Natural Bridge Rd., St.Louis, MO 63121-4499

I: mway@astro.princeton.edu

Received _____; accepted _____

arXiv:astro-ph/9708116v1 12 Aug 1997

¹Visiting Astronomer, Cerro Tololo Interamerican Observatory

²Visiting Astronomer, European Southern Observatory

²present address: Department of Astrophysical Science, Princeton University, Princeton,
NJ 08544

⁴Department of Astronomy and Astrophysics, P. Universidad Catolica de Chile, Casilla
104, Santiago 22 , Chile

⁵Presidential Chair in Science 1995

ABSTRACT

Using spectrophotometry of a large sample of galaxies in 19 Abell Clusters, we have selected 42 *candidate* AGN by the criteria used by Dressler et al. 1985 (DTS) in their analysis of the statistics of 22 AGN in 14 rich cluster fields, which are based on the equivalent width of [OII]3727Å, H β , and [OIII]5007Å emission. We have then discriminated AGN from HII region-like galaxies (hereafter HII galaxies) in the manner developed by Veilleux & Osterbrok 1987 (VO) using the additional information provided by H α and [NII]6583Å or H α and [SII]6716+6731Å emission, in order to test the reliability of the selection criteria used by DTS. We find that our sample is very similar to that of DTS before we discriminate AGN from HII galaxies, and would lead to similar conclusions. However, we find that their method inevitably mixes HII galaxies with AGN, even for the most luminous objects in our sample. Other authors have attempted to quantify the relative fraction of cluster to field AGN since the study of DTS (Hill & Oegerle 1993, Biviano et al. 1997) reaching similar conclusions, but using similar criteria to theirs to select AGN (or using the [OIII]5007Å/H β flux ratio test that also mixes HII galaxies with AGN). Our sample of true AGN is left too small to reach statistically meaningful conclusions, therefore a new study with the more time-consuming method that includes the other lines will be required to quantify the true relative fraction of cluster to field AGN.

Subject headings: clusters: galaxies: AGN

1. Introduction

The relative abundance of Emission Line Galaxies (ELG) in clusters and the field has been studied by many authors as a by-product of redshift surveys (Gisler 1978, DTS, Salzer et al. 1989, Hill & Oegerle 1993, Salzer et al. 1995, Biviano et al. 1997). ELG are found to be much less abundant in clusters, in agreement with the original observation by Osterbrok (1960) about ellipticals in the redshift survey of Humason et al. 1956. The early studies concluded that this could not be due entirely to the well known morphological segregation (Dressler 1980), but required an additional environmental effect. However, the recent study by Biviano et al. (1997) suggests that this is due to a magnitude bias and that correcting for it leaves relative abundances in agreement with morphological segregation alone, perhaps explaining the similar finding by Moss & Whittle (1993) which had a bright detection threshold.

A more difficult problem in these studies is to separate the galaxies with Active Galactic Nuclei (AGN) or Low Ionization Nuclear Emission Region (LINER) (both believed to be ionized by non-stellar, power-law spectra) from those with spectra of the type of HII hot-spots in actively star-forming regions in nearby galaxies (see e.g. Osterbrock 1989). A fairly clean separation is possible if the [NII]6583Å, [SII]6716+6731Å and [OI]6300Å lines can be detected, as was shown by VO with their suite of line-ratio tests based on the earlier work of Baldwin et al. (1981). Unfortunately, redshift surveys typically cover the wavelength range $\sim 3500\text{-}6500\text{\AA}$ where the lines cannot be detected. Therefore, the studies that have attempted to quantify the cluster to field ratio of AGN/LINERs have attempted a separation based on the equivalent width W of the [OIII]5007Å, [OII]3727Å and $H\beta$ emission lines, following Heckman 1980. If $W_{[\text{OIII}]5007} \gtrsim W_{[\text{OII}]3727}$ or $W_{H\beta} \gtrsim W_{[\text{OII}]3727}$, and $W_{[\text{OIII}]5007} \gtrsim W_{H\beta}$, the galaxy was classified as an AGN (DTS, Hill & Oegerle 1993). Biviano et al (1997) use a criterion of [OIII] to $H\beta$ flux ratio, which was originally thought

to be a reliable indicator of AGN (Shuder & Osterbrok 1981). Gisler (1978) used the Markarian lists to get AGN-type objects, but many of these are actually HII galaxies (VO). None of these methods selects AGN/LINERs reliably (Baldwin et al. 1981, VO). First, AGN and HII regions can be cleanly separated by measuring *flux* ratios for different pairs of lines. The $W_{[OIII]\lambda 5007} \gtrsim W_{H\beta}$ criterion translates into a genuine requirement of larger $[OIII]/H\beta$ flux ratio *because these lines are very close to one another* and, therefore, have the same underlying continuum. The other two criteria, however, involve widely separated lines which may differ in W *because of differing continua*, not differing fluxes, unless $W \gg 1$ for both lines. Second, even if the equivalent width ratios measured flux ratios, the requirement that $[OIII]\lambda 5007 \gtrsim H\beta$ and $[OIII]\lambda 5007 \gtrsim [OII]\lambda 3727$ is satisfied by *both* AGN and HII regions. It is not clear that the requirement $W_{H\beta} \gtrsim W_{[OII]\lambda 3727}$ is not satisfied by HII regions given the small number of HII regions in the study of Heckman 1980. It must also be mentioned that in comparing lines such as $[OII]\lambda 3727$ and $[OIII]\lambda 5007$ one must take into account the slit position angle and atmospheric differential refraction (see Filippenko 1982) which can place more flux in one line versus another simply due to the position of the slit on the sky. This effect is stronger when lines are widely separated *unlike* $H\beta$ and $[OIII]\lambda 5007$.

We have attempted, however, to calibrate the technique of equivalent widths by selecting it candidate AGN from a large sample of galaxies in 19 Abell Clusters for which spectra were obtained as part of a redshift survey. We have used the criteria used by DTS to identify 42 it candidate objects. Using 3 nights in 1993 on the ESO 2.2 meter and 4 nights in 1995 at the CTIO 1.5m we obtained flux calibrated spectra covering the wavelength range 4200–7500Å for our 42 it candidate AGN. By measuring accurate ratios of $[OIII]\lambda 5007/H\beta$, $[SII]\lambda 6716+6731/H\alpha$ and $[NII]\lambda 6583/H\alpha$ we have then separated AGN/LINERs from HII galaxies using the criteria developed by VO. We find that no threshold in equivalent width can cleanly separate them. We do not find it possible to separate them by an absolute

luminosity threshold either, contrary to what DTS argued: our AGN/LINERs and HII galaxies are mixed at all luminosities, in agreement with studies of nearby ELG that also find quite luminous HII galaxies (Ho 1996, Gallego et al. 1997). Thus, it is fair to say that the relative fraction of cluster to field AGN is not presently known, as our study is left with too small a sample to reach statistically sound conclusions. A study with the more time-consuming method that includes the other lines will be required to address this question, but a step in the right direction is the recent study of *field* AGN based on the CFRS (Tresse et al. 1996).

We present the observations and data reduction for the 42 it candidate AGN in the next section, and then the analysis of the reduced data in the subsequent section. Finally, we close with a section of discussion of the analysis, and the conclusions we draw from it. We use a Hubble constant $H_0 = 100 h$ km/s/Mpc.

2. Observations and Reductions

We started by selecting *candidate* AGN from a large set of ELG spectra obtained as part of a redshift survey in the field of 19 Abell Clusters (see Quintana et al. 1997, Way et al. 1997, Quintana et al. 1996), using the criteria of DTS for selection. Spectra for these objects, covering the wavelength range $\sim 4200\text{--}7500\text{\AA}$, were then obtained from two different observing runs.

The first run was at the ESO-MPI 2.2 meter telescope using EFOSC2 on the 2 nights of October 18 and 19, 1993. The set up was with CCD #19, a 1024X1024 Thompson chip with $19\mu\text{m}$ pixels which has a gain of $2e^-/\text{ADU}$ with readout noise of $<5e^-$. Grism #6 with 300 lines/mm blazed at 5000\AA and a dispersion of $\sim 2.7\text{\AA}/\text{pixel}$, and a $1.5''$ slit. This yielded a resolution of $\sim 9\text{\AA}$ FWHM and a wavelength coverage of $\sim 4600\text{--}7200\text{\AA}$.

The second run was on the CTIO 1.5 meter telescope using the the Cassegrain focus Boller and Chivens spectrograph on the 4 nights of November 29 to December 2, 1995. A Loral 1200X800 CCD was used which has $15\mu\text{m}$ pixels. Gain was set to $1\text{e}^-/\text{ADU}$ which as a read noise of 5.88e^- . Grating #32 was used which has 300 lines/mm blazed at 6750\AA giving a wavelength coverage of $\sim 3450\text{\AA}$. This in turn gave us excellent sensitivity in the $4200\text{-}7500\text{\AA}$ range used and a dispersion of $\sim 2.8\text{\AA}/\text{pixel}$. $4.5'' = 221.2\mu\text{m}$ and $4.0'' = 221.2\mu\text{m}$ slits were used for object exposures. These gave resolutions of $\sim 8\text{-}9\text{\AA}$ FWHM. Helium, Neon, and Argon lamps were also used to generate comparison frames for wavelength calibrating the data. See Table 1 for a summary of telescope and instrument properties.

Six spectra were obtained from the ESO 2.2 meter run and another forty from the CTIO 1.5 meter. Some objects were observed more than once and, when appropriate, the spectrum of better S/N was selected for the analysis described in the next section. The spectra were calibrated with the spectrophotometric standards of Baldwin & Stone (1984) and Hamuy et al. (1992). Spectrophotometric standards were taken several times over the course of the night to assure good airmass coverage. Three equal length exposures were taken of each object. Each set of 3 exposures were later combined with a median filter to eliminate cosmic rays using the IRAF COMBINE task.

The reduction of each data run was basically the same. Since we used the IRAF (Tody

Table 1. Spectra Observed

Telescope	CCD	e^-/ADU	Read Noise e^-	Blaze(\AA)	l/mm	$\text{\AA}/\text{pixel}$	Res(\AA)	Range(\AA)
ESO 2.2m	1024 ² Thompson	2	5	5000	300	2.7	9	4600-7200
CTIO 1.5m	1200X800 Loral	1	5.88	6750	300	2.8	8-9	4200-7500

1993) software package to reduce our data we had to update the EFOSC2 fits headers with some additional information required by IRAF. Bias images were summed with the ZEROCOMBINE task, flat-fields with FLATCOMBINE, and each of the three object copies with the COMBINE task using a median filter to rid them of cosmic rays. Using the RESPONSE task the combined flat-field was then fit with a 6th order spline to fit inherent large scale features. CCDPROC was then used to bias and flatfield correct the object spectra and spectrophotometric standards. Afterwards CTIOSLIT was used to extract the object and spectrophotometric standard spectra from the ccd frames. It then uses the spectrophotometric standards to correct the object spectra for extinction and flux. Not all of our data was successfully flux calibrated (due to some non-photometric weather), but for the purposes of this paper they are more than adequate. This is because the emission lines we wish to measure are ratioed with respect to close neighboring lines, and therefore the shape of the underlying continuum is not crucial, e.g. $H\beta$ and $[OIII]5007\text{\AA}$ or $H\alpha$ and $[NII]6583\text{\AA}$.

An automated task in IRAF called FITPROFS was used to measure the flux within the desired line profiles. This task allows one to set the region about the line from which it can pick the continuum. The continuum is then fit with a linear function in the region under the line we want to measure. Once the region is chosen, one also inputs the center of the line to be measured, and a gaussian was chose to fit the line profile with. To estimate the error in the emission line fit one must estimate the uncertainty of a pixel in the line profile (which is what FITPROFS requires in one of it's parameters). This can be obtained by estimating the RMS on a piece of the spectrum free of emission or absorbtion lines (or else a sigma clipping of any emission or absorbtion lines).

3. Analysis

The basic data for our it candidate AGN, before classifying them by the diagnostic diagrams constructed from the data described in section 2, are presented in Table 2. They were selected from the ELG spectra of a redshift survey in the field of 19 Abell Clusters that are representative of clusters of richness $R \geq 1$ in the Abell catalog, and therefore similar to the cluster sample of Dressler & Shechtman (1988) used by DTS. The sole exception is A133, which is a $R = 0$ cluster, but whose velocity dispersion is more like that of a $R = 1$ cluster (Way et al. 1997).

The range of absolute magnitudes of our it candidate AGN is similar to that of the DTS sample, and so is the distribution of magnitudes. The main difference is that our objects are distributed out to much larger distances. Given the similarities of the two samples, it seems fair to conclude that we have been successful at obtaining a sample very similar to that of the DTS study. It is not surprising, then, that the fraction of candidates in and out of clusters are rather similar: here 64% and 36% respectively, compared to 59% and 41% in the DTS study. If A133 were not included on account of being a $R = 0$ cluster, then our sample becomes even more like the DTS sample, with the percentages above changing to 60% and 40% for our sample. Thus, *we would have been lead to the same conclusions with regards to the relative fraction of cluster to field AGN of the many studies that have identified AGN in a manner that does not fully separate them from HII galaxies.*

We can now turn to the analysis of our longer wavelength data to separate AGN/LINERs from HII galaxies. The basic data obtained from the reduction described in section 2 are presented in Table 3, and the tabulated flux ratios are plotted in the diagnostic diagrams of VO in Figure 1. The dashed line in each diagram is the line that VO found to provide a good empirical separation of nearby AGN/LINERs and HII regions, and we shall use it here to distinguish AGN/LINERs from HII galaxies in our sample. Tresse et

al. (1997) use an extreme theoretical model to obtain an upper limit to the HII boundary in the diagnostic diagrams which differs significantly from the VO empirical boundaries for $[\text{OIII}]/\text{H}\beta \lesssim 3$. However, for the diagnostic diagram that can be compared directly (Fig. 1(b)), we find that this would affect only a few of the objects we have classified as transitional or uncertain anyway. Our flux ratios are not corrected for reddening, but such a correction is small for the lines chosen in the diagnostic diagrams (VO). We have not corrected for stellar absorption under the Balmer lines either, although this is a more substantial correction. Since this only moves the objects down and a bit to the left in the diagrams, it can only decrease the number of AGN/LINERs in our sample and, therefore, not affect our main conclusion that blue-spectra based studies of AGN using equivalent width selection criteria (or $[\text{OIII}]/\text{H}\beta$ flux ratio) get a large “contamination” from HII galaxies. There are sizeable errors associated with some of our flux ratios. This is because the lines are fairly weak in some of the objects, and some of the lines are weak in nearly all of the objects. For clarity, we show separately in Figure 2 the same diagnostic diagrams of Fig. 1 with our estimate of 1σ errors. Note that despite the substantial errors, most of the points stay entirely on the same side of the empirical dividing line. Therefore, we conclude that a large number of our objects do have spectra characteristic of HII galaxies.

On the basis of the diagnostic diagrams, Fig. 1, we have classified the galaxies in our sample in two ways. First, a subjective classification based on inspection of the the distances of the flux-ratio data points to the empirical dividing lines, which we list in Table 3 for each of the diagnostic diagrams. The dividing lines can be moved, we estimate, by ± 0.1 without affecting the classifications of VO, therefore we consider the distance to be significant only if it exceeds 0.1 in absolute value. The identification is considered secure if all distances are of the same sign (unless they are all < 0.1), or if two distances are of the same sign, but the third is < 0.1 in absolute value. Objects for which two distances are large and of opposite sign make an object “transitional” or “uncertain”, unless the third distance is very much

larger. Not every object is consistently in the same region of each of the diagrams in Fig. 1, therefore we list the distance in Table 3 with an appropriate sign to indicate if the galaxy lies in the AGN/LINER (+) or HII galaxy (–) region in each of the diagrams. For the objects classified as AGN/LINER or HII galaxy we have inspected the individual spectra to make sure that they are consistent with the classification of the object. Second, we have also classified the objects by a simple, objective rule: if the sum of the distances, columns 6-8 of Table 3, exceeds 0.3, then the object is classified as an AGN/LINER or HII galaxy depending on the sign, and objects in between are classified as transitional. We show in Figure 3 the sum of the distances, column 9 of Table 3, plotted against recessional velocity, column 8 of Table 2. Filled squares are AGN/LINERS selected subjectively as explained above, open squares are transitional objects, and stars are HII-region objects. One can see that if we had classified galaxies with the objective criterion (dotted line) the results would have been essentially the same. Also, it is apparent in the figure that we do not have systematic effects related to distance affecting our classifications.

Our final classification, listed in column 10 of Table 3, is based on the objective criterion, but with the ± 0.1 uncertainty treated as statistical. Thus, if the sum of the distances, column 9 of Table 3, is $\Sigma d_i > \sqrt{3} \times 0.1$ ($\Sigma d_i < -\sqrt{3} \times 0.1$, $-\sqrt{3} \times 0.1 < \Sigma d_i < \sqrt{3} \times 0.1$), we have classified the object as an AGN/LINER (HII galaxy, transitional) and denoted them as S/L (HII, T) in Table 3. This does not change at all the number of objects that are classified as AGN/LINERS. Two objects (C3141-34 and C3864-5b) had to be classified differently because of undetectable flux in some lines. C3141-34 had no detectable [NII] and [SII] lines, but it was detected in $H\alpha$. Therefore it clearly belongs in the HII category given its [OIII]/ $H\beta$ flux ratio, and this is confirmed by the observed [OI]/ $H\alpha$ ratio. C3864-5b was not detected in $H\beta$, but for any [OIII]/ $H\beta$ flux ratio the other flux ratios put it in the AGN/LINER region. All but one transitional objects have two distances of opposite sign making a small Σd_i . It may be that these are objects in which there is star

formation surrounding a LINER (see Ho 1996; the exact definition of “transitional” is not the same), which would be picked up because our slits cover a few kiloparsecs around the galaxy center. However, three of them have rather uncertain flux ratios and, therefore, it may be that the small Σd_i is due to noise.

With the classification assigned in Table 3, we have looked for equivalent width thresholds that might help distinguish AGN/LINERs from HII regions. However, no threshold in the equivalent width ratios $W_{[OIII]}/W_{[OII]}$ or $W_{H\beta}/W_{[OII]}$, and $W_{[OIII]}/W_{H\beta}$ can separate them. Likewise, we have tried to see if absolute luminosity can help distinguish them. Unfortunately, AGN/LINERs and HII galaxies in our sample remain mixed at all luminosities, even though the ratio of HII galaxies to AGN/LINERs indeed decreases with luminosity.

4. Discussion and Conclusions

The analysis of the previous section leaves us, unfortunately, with only 10 AGN/LINERs. Naturally, since our slits cover a few kiloparsecs around the galaxy centers, we cannot be sure that the emission from our AGN/LINERs is really from their nuclei. However, we are not aware of any detection of their type of spectra from non-nuclear regions in studies of nearby ELG. Our main conclusion is that blue-spectra based studies of AGN using equivalent width selection criteria (or $[OIII]/H\beta$ flux ratio) get a large “contamination” from HII galaxies, and therefore that the true relative fraction of cluster to field AGN is not known.

To the extent that both AGN and HII galaxies depend on the availability of gas for their existence, one might expect this ratio to be simply that determined from studies of ELG that do not separate between these classes. However, different spectral types are

found to be distributed differently as a function of radial distance in a detailed study of one cluster (Fisher et al. 1997). Another reason it would be interesting to separately study HII galaxies from AGN in clusters is that it would be possible to clarify if indeed some clusters have an abnormally high incidence of AGN (DTS), and thereby whether environmental effects are at work. Two of the clusters (A133 and A3194) in our sample show several *candidate* AGN ($\sim 5\%$ of the cluster galaxies), as was the case of one cluster in the DTS sample. However, in the case of A133 the flux ratio tests indicate that only one is (marginally) an AGN/LINER. In the case of A3194 all three *candidate* AGN turn out to be bona fide cluster AGN/LINERS, although one of them (C3194-7c) is rather far from the cluster center (at least $2.2h^{-1}$ Mpc). We cannot know, of course, if this is a high fraction of AGN for clusters without knowing the true abundance of AGN in clusters.

This work has been supported by an NSF grant and by Research and Research Board awards at The University of Missouri–St.Louis. One of us (RF) would like to acknowledge the hospitality of the Physics Department at UCSC while this work was being written, and D. Osterbrok for a useful discussion on AGN. This research has made use of NASA’s Extragalactic Database, ADS Abstract Service, and the Digitized Sky Survey at STScI. This project was partially supported by FONDECYT grants 8970009 and 7960004.

REFERENCES

- Baldwin, J.A., Phillips, M.M., and Terlevich, R. 1981 PASP 93, 5
- Baldwin, J.A., and Stone R.P.S. 1984 MNRAS 206, 241
- Biviano, A. et al. 1997 A&A 321, 84
- Dressler, A. 1980 ApJ 236, 351
- Dressler, A., Thompson, I. and Shechtman, S. 1985 ApJ 288, 481
- Dressler, A., and Shechtman, S. 1988 AJ 95, 284
- Filipenko, A.V. 1982 PASP 94, 715
- Filipenko, A.V. and Terlevich, R. 1992 ApJ 397, L79
- Fisher, D. et al 1997, presented at the “Clusters of Galaxies at Different Redshifts”, May 27-31, Ruidoso, New Mexico
- Gallego, J. et al. 1997 ApJ 475, 502
- Gisler, G.R. 1978 MNRAS 183, 633
- Hamuy, M. et al. 1992 PASP 104, 533
- Heckman, T.M. 1980 A&A 87, 152
- Hill, J.M. and Oegerle, W.R. 1993 AJ 106, 831
- Ho, L.C. 1996, “Optical Spectroscopy of LINERs and Low Luminosity Seyfert Nuclei” in The Physics of LINERs in View of Recent Observations, A.S.P. Conference Ser., Vol 103, eds. M. Eracleous et al., 103 (astro-ph/9605190)
- Hubble, E., Humason, M.L. 1931 ApJ 74, 43

- Humason, M.L., Mayall, N.U. and Sandage, A.R. 1956 ApJ 61, 97
- Moss, C. and Whittle, M. 1993 ApJ 407, L17
- Osterbrock, D.E. 1960 ApJ 132, 325
- Osterbrock, D.E. 1989 *Astrophysics of Gaseous Nebulae and Active Galactic Nuclei* (Mill Valley: University Science Books)
- Quintana, H., Ramirez, A. and Way, M.J. 1996 AJ 112, 36
- Quintana, H., Infante, L. and Way, M.J. 1997 in preparation
- Salzer, J. J. et al. 1989 ApJS 70, 479
- Salzer, J. J. et al. 1995 AJ 109, 2376
- Shuder, J.M. and Osterbrock, D. E. 1981 ApJ 250, 55
- Spitzer, L. and Baade, W. 1951 ApJ 113, 413
- Tody, D. 1993, “IRAF in the Nineties” in *Astronomical Data Analysis Software and Systems II*, A.S.P. Conference Ser., Vol 52, eds. R.J. Hanisch, R.J.V. Brissenden, and J. Barnes, 173
- Tresse, L. et al. 1996 MNRAS 281, 847
- Veilleux, S. and Osterbrock, D. E. 1987 ApJS 63, 295
- Way, M.J., Quintana, H., and Infante, L. 1997, submitted to AJ

Table 2. Objects Observed

ID ⁽¹⁾	α (1950) ⁽²⁾	δ (1950) ⁽²⁾	mag ⁽³⁾	$W_{[OII]}$ ⁽⁴⁾	$W_{H\beta}$ ⁽⁴⁾	$W_{[OIII]}$ ⁽⁴⁾	v_{\odot} ⁽⁵⁾	Mag ⁽⁶⁾	R ⁽⁷⁾	Memb ⁽⁸⁾
C2854-74	1:00:15	-51:17:57.1	16.2	5.273	9.942	8.306	21074	-21.9	1	N
C487-51	4:21:34	-24:13:32.3	15.1	34.49	7.938	85.94	17726	-22.6	1	N
C3194-28	3:57:20	-30:20:38.3	16.1	33.91	1.278	52.4	29278	-22.7	2	Y
C3194-7c	3:55:13	-30:26:53.6	16.6	38.73	2.229	8.386	28692	-22.2	2	Y
C3194-31	3:57:09	-30:26:39.8	16.4	146.3	7.511	50.26	27895	-22.3	2	Y
C3264-4d	4:27:28	-49:16:53.5	16.3	75.51	11.85	42.4	29047	-22.5	1	Y
C3264-5e	4:27:16	-49:18:04.4	17.7	49.17	39.71	91.31	31900	-21.3	1	N
C2854-45	0:58:07	-50:32:59.2	17.2	100.9	96.90	110	18719	-20.7	1	Y
C2854-68	0:58:06	-50:55:33.3	17.1	34.35	12.07	20.43	19144	-20.8	1	Y
C3153-67	3:36:51	-34:38:05.4	16.7	8.411	18.57	28.8	37184	-22.7	1	Y
C3153-29	3:41:19	-34:42:58.3	16.4	8.036	4.425	10.99	37536	-23.0	1	Y
C3223-46	4:01:56	-30:13:36.8	17.1	22.86	3.88	13.82	18246	-20.7	2	Y
C3223-6a	4:01:14	-30:35:49.5	17.0	6.763	3.112	2.925	18193	-20.8	2	Y
C3223-14	4:03:30	-30:26:13.3	17.4	25.62	3.203	10.59	17573	-20.3	2	Y
C3223-01	4:02:43	-30:01:31.8	17.3	15.55	14.0	41.69	17909	-20.5	2	Y
C487-38	4:22:06	-24:51:48.4	17.6	26.05	4.322	12.29	17268	-20.1	1	N
C2871-6c	1:04:58	-37:02:12.4	15.8	24.54	3.584	27.44	3932	-18.7	2	N
C3921-0d	22:48:51	-64:09:56.0	17.2	36.58	13.28	25.59	31999	-21.8	2	N
C2871-53	1:05:19	-36:59:02.0	17.1	13.08	13.30	10.06	35870	-22.2	2	Y
C2923-71	1:30:48	-31:51:41.8	17.6	39.34	9.348	28.87	25540	-20.9	1	N
C3142-53	3:34:49	-39:43:22.4	17.4	9.494	4.718	2.40	21509	-20.8	1	N
C3142-08	3:35:13	-39:39:43.3	17.5	40.97	10.83	30.62	17530	-20.2	1	N
C3223-26	4:04:05	-30:32:32.0	15.9	5.876	2.495	1.225	17613	-21.8	2	Y
C3188-62	3:55:40	-27:17:52.0	17.4	24.52	10.02	24.99	21447	-20.8	1	N
C3188-16	3:57:07	-27:12:16.8	17.3	33.83	4.079	17.67	18772	-20.6	1	Y
C3141-33	3:34:01	-28:54:45.0	17.6	8.839	0.7968	13.39	30721	-21.3	1	Y
C3864-5b	22:12:52	-52:45:32.0	17.1	9.28	0.0	10.56	15936	-20.4	1	N
C3112-0b	3:16:43	-44:30:21.3		64.21	18.40	80.49	22582		2	Y
C2911-75	1:24:02	-38:27:53.6	17.5	41.08	6.678	17.26	24201	-20.9	1	Y
C3112-25	3:16:27	-44:49:55.3		10.20	5.694	2.768	20085		2	N
C3141-04	3:35:07	-27:36:04.6	17.8	24.30	3.599	11.29	31338	-21.2	1	Y
C3141-34	3:34:29	-28:50:18.3	17.8	0.0	25.76	8.082	38857	-21.7	1	N
C3151-06	3:40:54	-28:38:12.7	17.0	55.46	7.753	17.06	20777	-21.1	1	Y
C3151-14	3:38:48	-28:51:54.8	16.8	47.65	12.26	23.01	17778	-21.0	1	N
C3266-12	4:32:52	-61:04:44.5		11.30	2.10	6.30	18193		2	Y

Table 2—Continued

ID ⁽¹⁾	α (1950) ⁽²⁾	δ (1950) ⁽²⁾	mag ⁽³⁾	$W_{[OII]}$ ⁽⁴⁾	$W_{H\beta}$ ⁽⁴⁾	$W_{[OIII]}$ ⁽⁴⁾	v_{\odot} ⁽⁵⁾	Mag ⁽⁶⁾	R ⁽⁷⁾	Memb ⁽⁸⁾
C3223-78	4:05:30	-31:42:19.35	17.3	58.98	13.45	31.02	21104	-20.8	2	N
E3266-03	4:33:58	-61:00:14.8		7.80	3.27	13.59	17671		2	Y
E133-29	0:59:40	-22:22:25.3	16.1	12.55	2.70	26.35	16403	-21.5	0	Y
E133-30	0:59:46	-22:08:16.2	15.9	12.20	1.82	15.10	16315	-21.7	0	Y
E133-12	1:01:40	-21:53:04.3	16.5	9.00	4.40	3.66	16228	-21.0	0	Y
E133-33	0:59:41	-22:20:49.3	18.1	6.93	3.10	2.10	15619	-19.4	0	Y
E119-08	0:56:14	-01:21:59.7	15.7R	18.48	4.07	41.57	13935	-21.5R	1	Y

⁽¹⁾Object identification: prefix (E = ESO 1993 run, C=CTIO 1995 run) followed by Abell cluster number and a fiber id number from redshift survey.

⁽²⁾Right ascension (α) and declination (δ).

⁽³⁾Apparent magnitude in V, except for one available only in R; some are not available.

⁽⁴⁾Equivalent width, in Å, for [OII] ($H\beta$, [OIII]) line (from redshift survey fiber spectra).

⁽⁵⁾Heliocentric recession velocity, in km/s.

⁽⁶⁾Absolute magnitude in V for $h = 0.5$ as in DTS.

⁽⁷⁾Cluster richness class.

⁽⁸⁾Membership in cluster based on velocity distribution, as in DTS.

Table 3. Diagnostic Flux Ratios

ID ⁽¹⁾	$\frac{[\text{NII}]}{\text{H}\alpha}$ ⁽²⁾	$\frac{[\text{SII}]}{\text{H}\alpha}$ ⁽²⁾	$\frac{[\text{OIII}]}{\text{H}\beta}$ ⁽²⁾	$\frac{[\text{OI}]}{\text{H}\alpha}$ ⁽²⁾	$d_{[\text{NII}]}$ ⁽³⁾	$d_{[\text{SII}]}$ ⁽³⁾	$d_{[\text{OI}]}$ ⁽³⁾	Σd_i ⁽⁴⁾	Class ⁽⁵⁾	r (') ⁽⁶⁾
C2854-74	-0.1979	-1.1465	0.0244	-1.6831	0.0509	-.7113	-.4572	-1.1176	HII	39
C487-51	0.0064	-0.2926	1.0640	-1.1020	0.6285	0.4971	0.4503	1.5759	S/L	16
C3194-28	0.0765	-0.1329	1.3320	-0.8865	0.8557	0.7922	0.7740	2.4219	S/L	3
C3194-7c	0.1200	0.1027	0.6504	-0.9782	0.5167	0.6581	0.3944	1.5692	S/L	31
C3194-31	-0.0068	-0.0358	0.6523	-0.8139	0.4010	0.5285	0.5501	1.4796	S/L	8
C3264-4d	-0.7483	-0.3626	0.3858	-1.4202	-.3810	0.1332	-.1086	-0.3564	HII	40
C3264-5e	-1.1287	-0.7455	0.6949	-1.0142	-.3753	-.0870	0.3757	-0.0870	T	43
C2854-45	-0.8767	-0.4712	0.3053	-1.1397	-.5326	0.0065	0.1363	-0.3898	HII	17
C2854-68	-0.8104	-0.4199	0.1774	-1.4684	-.5216	0.0299	-.2135	-0.7052	HII	11
C3153-67	-0.1349	-0.7997	0.4898	-1.3594	0.2204	-.2405	-.0180	-0.0381	T	36
C3153-29	-0.2001	-0.7859	0.3038	-1.9484	0.0974	-.2949	-.6351	-0.8326	HII	38
C3223-46	-0.6998	-0.3880	0.3638	-1.3326	-.3491	0.1025	-.0319	-0.2785	HII	82
C3223-6a	-0.2537	-0.2649	0.4659	-1.2803	0.1011	0.2506	0.0487	0.4004	S/L	83
C3223-14	-1.0770	-0.4298	0.4739	-0.8013	-.5471	0.0973	0.5078	0.0580	T	56
C3223-01	-0.2196	-0.6494	0.5407	-1.5666	0.1612	-.0826	-.1946	-0.1160	T	80
C487-38	-0.8258	-0.2322	0.2806	-1.2759	-.4984	0.2332	-.0009	-0.2661	HII	37
C2871-6c	-0.8397	-0.4264	0.3076	-1.2380	-.4993	0.0503	0.0422	-0.4068	HII	10
C3921-0d	-0.8324	-0.4774	0.0637	-1.4240	-.5741	-.0425	-.1956	-0.8122	HII	46
C2871-53	-0.4386	-0.9343	-0.1271	-1.3006	-.2013	-.5156	-.1077	-0.8246	HII	4
C2923-71	-0.6897	-0.5551	0.3586	-0.4273	-.3422	-.0585	0.8404	0.4397	S/L	33
C3142-53	-0.4091	-0.5468	-0.1061	-1.1723	-.1705	-.1277	0.0218	-0.2764	HII	15
C3142-08	-0.5680	-0.5819	0.5168	-1.4641	-.1585	-.0299	-.1073	-0.2957	HII	19
C3223-26	-0.3155	-0.6981	-0.0608	-1.3718	-.0737	-.2746	-.1674	-0.5157	HII	45
C3188-62	-0.6692	-0.3550	0.7318	-1.0153	-.0978	0.2653	0.3876	0.5551	S/L	7
C3188-16	-0.7074	-0.3883	0.3263	-1.4281	-.3716	0.0920	-.1341	-0.4137	HII	21
C3141-33	-0.0944	-0.3770	1.1109	-1.5080	0.5809	0.4629	0.1353	1.1791	S/L	44
C3864-5b	0.2815	-0.1282		-0.0893				>1.75	S/L	62
C3112-0b	-1.0281	-0.7460	0.6580	-1.9838	-.3617	-.1094	-.5126	-0.9837	HII	9
C2911-75	-0.9670	-0.5264	0.3438	-1.4773	-.5809	-.0357	-.1759	-0.7925	HII	14
C3112-25	-0.3402	-0.5732	-0.3764	-1.7861	-.1173	-.1725	-.6263	-0.9161	HII	25
C3141-04	-0.6283	-0.4655	0.0600	-1.0901	-.3728	-.0311	0.1309	-0.2730	HII	37
C3141-34			-0.4162	-1.8316			-.6769		HII	38
C3151-06	-0.9735	-0.3411	0.7438	-0.8557	-.2603	0.2831	0.5414	0.5642	S/L	40
C3151-14	-0.8660	-0.5877	0.4450	-1.2858	-.4382	-.0611	0.0369	-0.4624	HII	6
C3266-12	-0.2505	-0.4134	0.2764	-1.3456	0.0413	0.0554	-.0693	0.0274	T	47

Table 3—Continued

ID ⁽¹⁾	$\frac{[\text{NII}]}{\text{H}\alpha}$ ⁽²⁾	$\frac{[\text{SII}]}{\text{H}\alpha}$ ⁽²⁾	$\frac{[\text{OIII}]}{\text{H}\beta}$ ⁽²⁾	$\frac{[\text{OI}]}{\text{H}\alpha}$ ⁽²⁾	$d_{[\text{NII}]}$ ⁽³⁾	$d_{[\text{SII}]}$ ⁽³⁾	$d_{[\text{OI}]}$ ⁽³⁾	Σd_i ⁽⁴⁾	Class ⁽⁵⁾	r (′) ⁽⁶⁾
C3223-78	-0.8164	-0.5135	0.3096	-1.3439	-.4776	-.0331	-.0586	-0.5693	HII	48
E3266-03	-0.1366	-0.2371	1.0840	-0.6779	0.5315	0.5532	0.8358	1.9205	S/L	63
E133-29	-0.2388	-0.6129	0.9500	-2.0615	0.3665	0.1806	>-.4284	0.1187	T	20
E133-30	-0.1661	-0.3583	0.9886	-2.1787	0.4470	0.3989	>-.5334	0.3125	S/L	8
E133-12	-0.4133	-0.5030	-0.2431	-2.1696	-.1833	-.0940	-.9842	-1.2615	HII	25
E133-33	-0.3738	-0.4022	-0.2557	-1.7467	-.1446	0.0059	-.5686	-0.7073	HII	19
E119-08	0.1194	0.1324	1.2810	-0.7206	0.8539	0.9675	0.8891	2.7105	S/L	38

⁽¹⁾Object identification, as in Table 2.

⁽²⁾Logarithm of [NII]/H α ([SII]/H α , [OIII]/H β , [OI]/H α) flux ratio.

⁽³⁾Distance from dividing line in the [OIII]/H β vs. [NII]/H α ([SII]/H α , [OI]/H α) diagnostic diagram, Fig. 1a (1b, 1c).

⁽⁴⁾Sum of distances in columns 6, 7 and 8.

⁽⁵⁾Final classification; see text.

⁽⁶⁾Projected distance from cluster center, in minutes of arc.

Fig. 1.— Diagnostic diagrams for our *candidate* AGN, showing the logarithm of the [OIII]/H β flux ratio vs (a) [NII]/H α , (b) [SII]/H α and (c) [OI]/H α flux ratios. The dashed line in each diagram is the empirical dividing line separating AGN/LINERs from HII-regions and HII-region-like galaxies in the study of VO.

Fig. 2.— Same as Figure 1, with 1σ error bars added.

Fig. 3.— Comparison of the two classifications discussed in the text. The quantity Σd_i (column 9 of Table 3) is plotted against the recession velocity (column 8 of Table 2) for each galaxy. The filled squares (open squares, stars) are those classified as AGN/LINERs (transitional, HII galaxy) based on the subjective criterion discussed. The dotted line marks a possible separation based simply on Σd_i (see text).

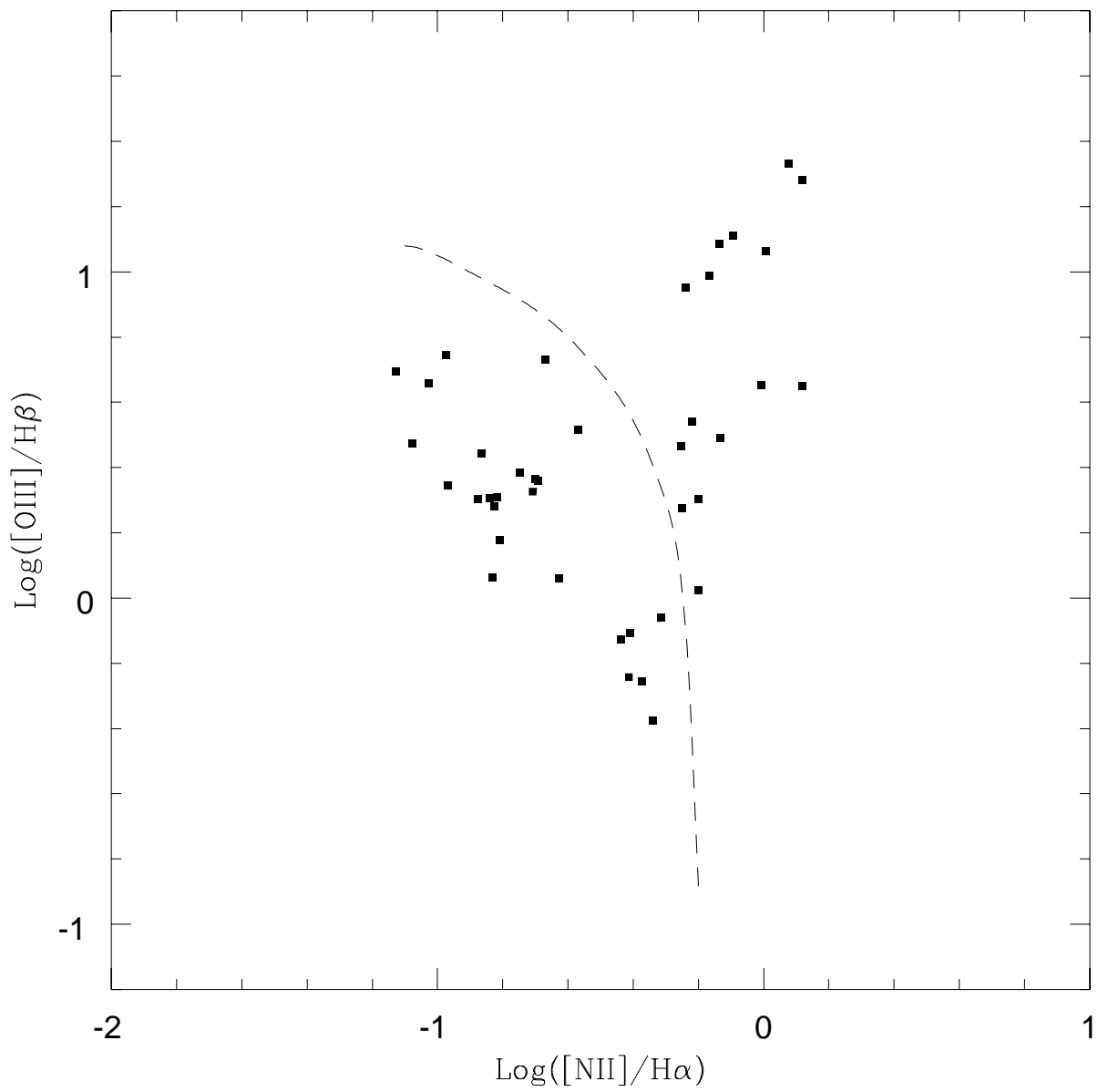


Figure 1(a)

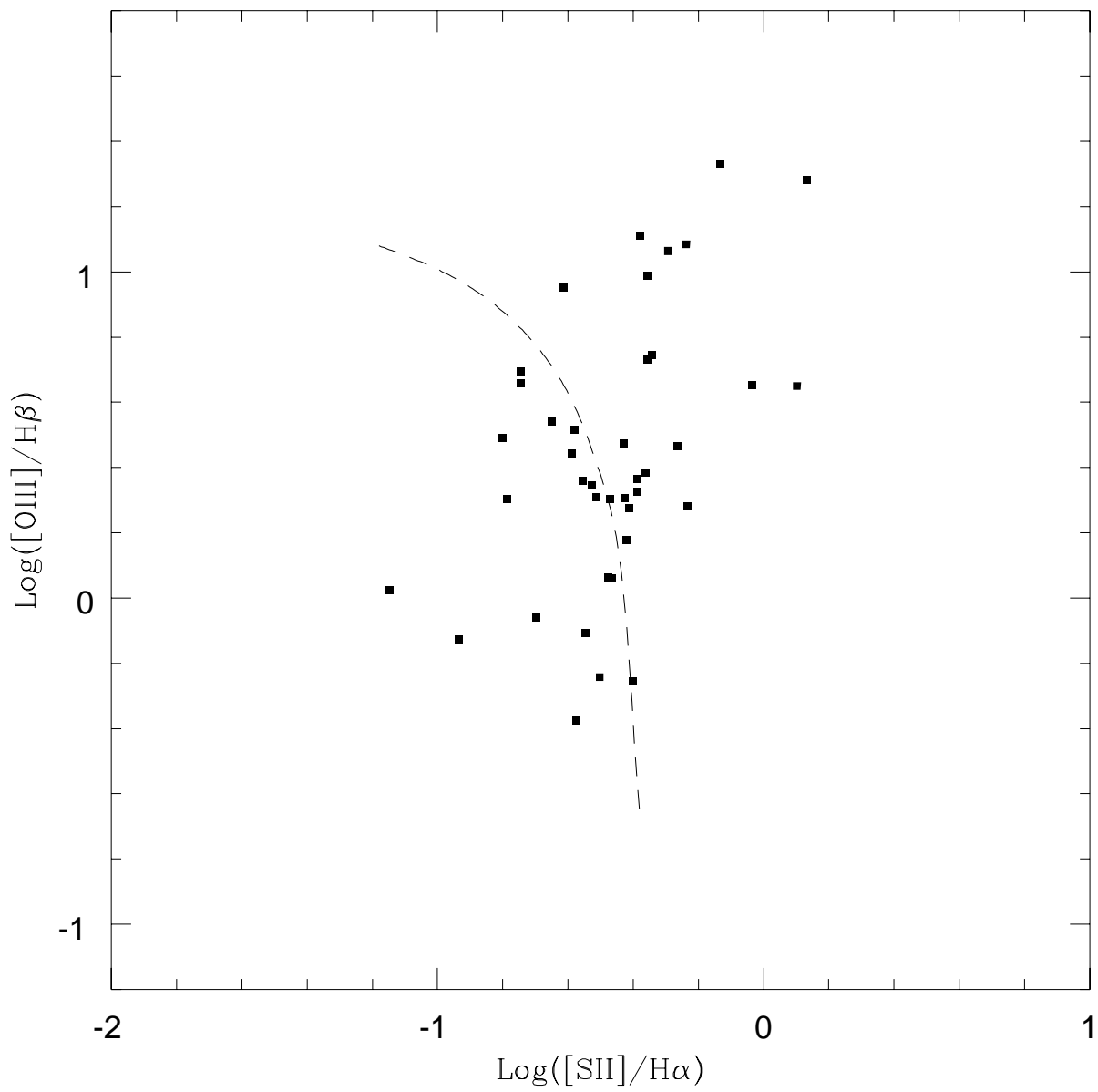


Figure 1(b)

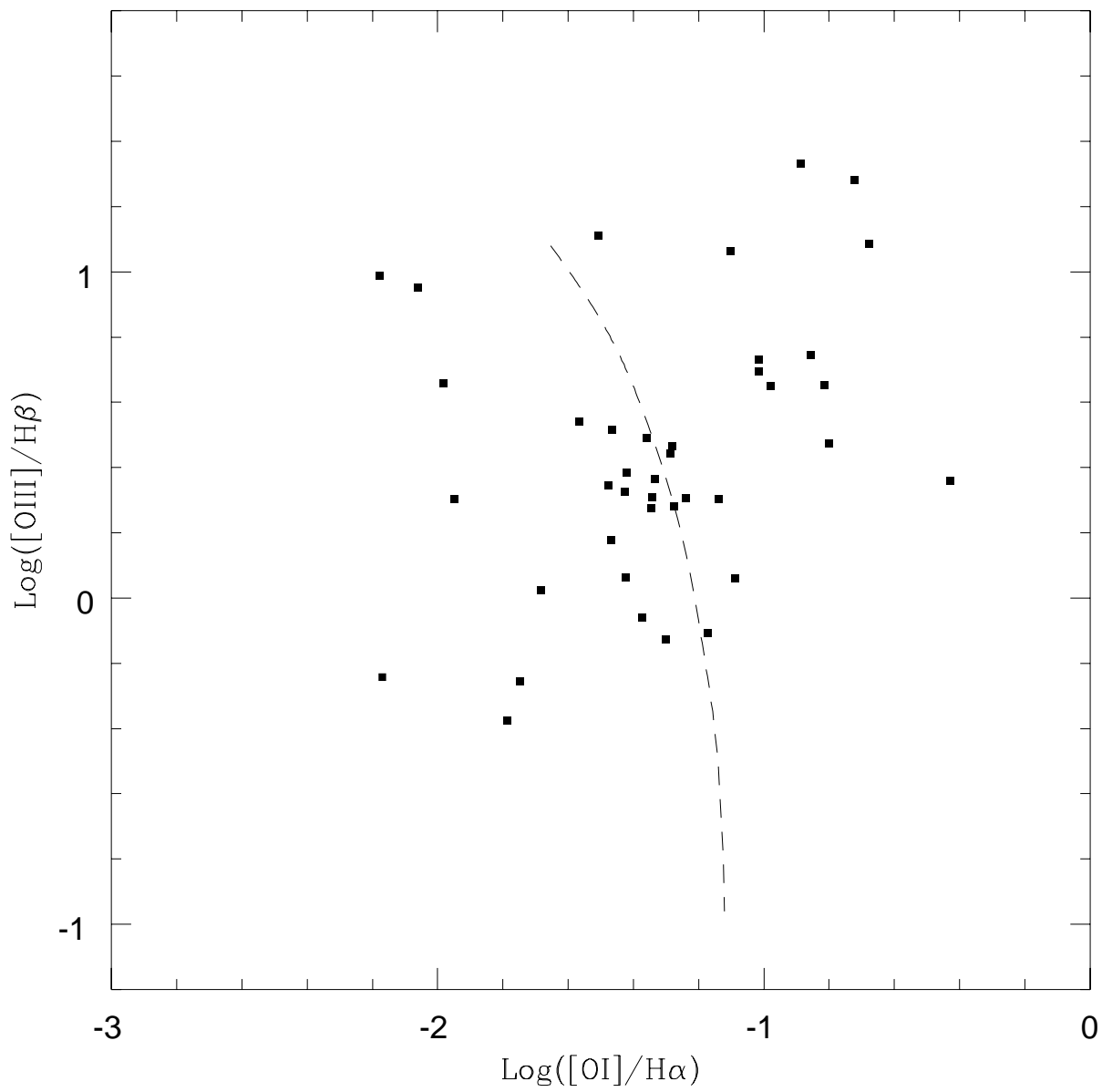


Figure 1(c)

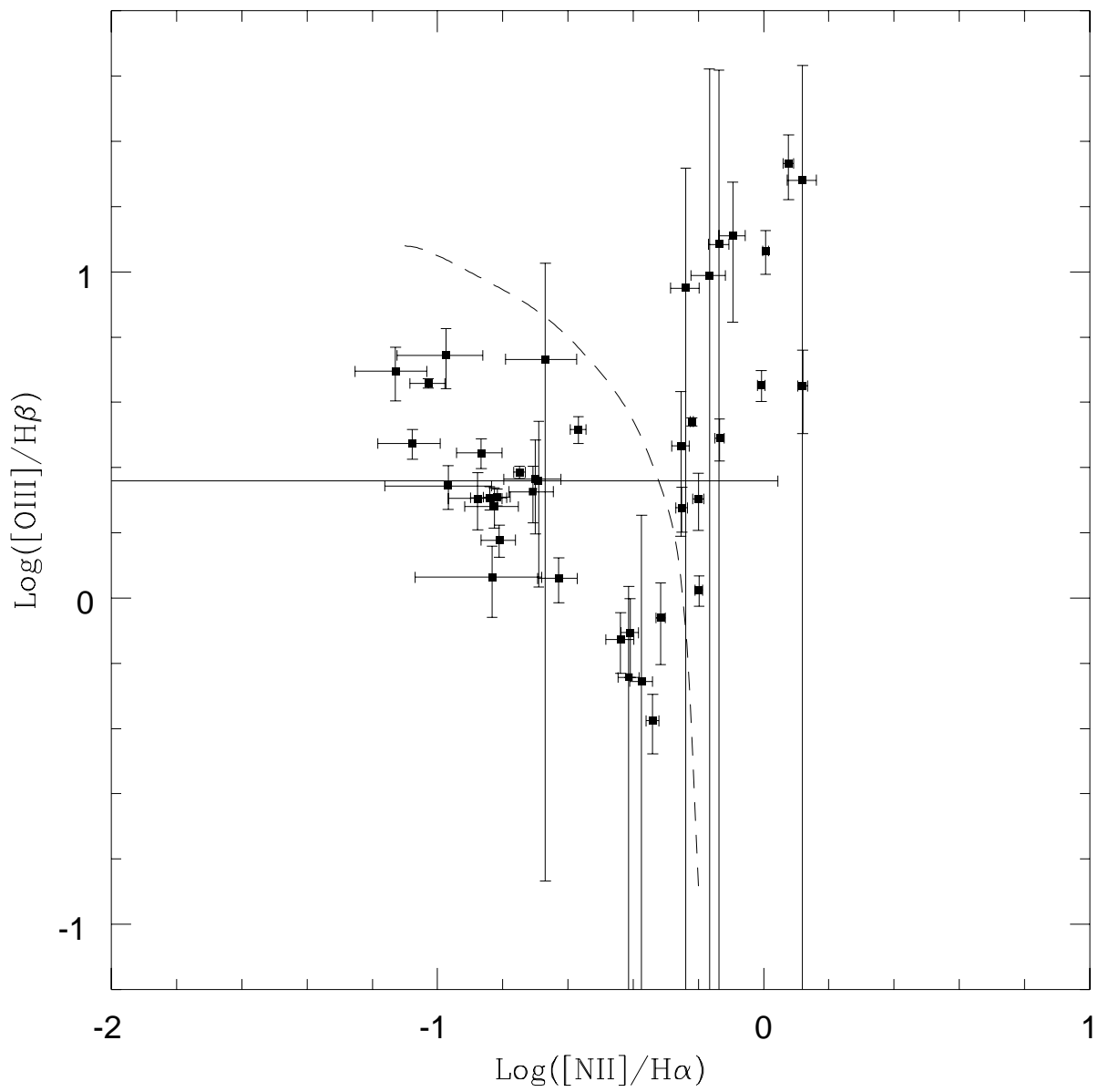


Figure 2(a)

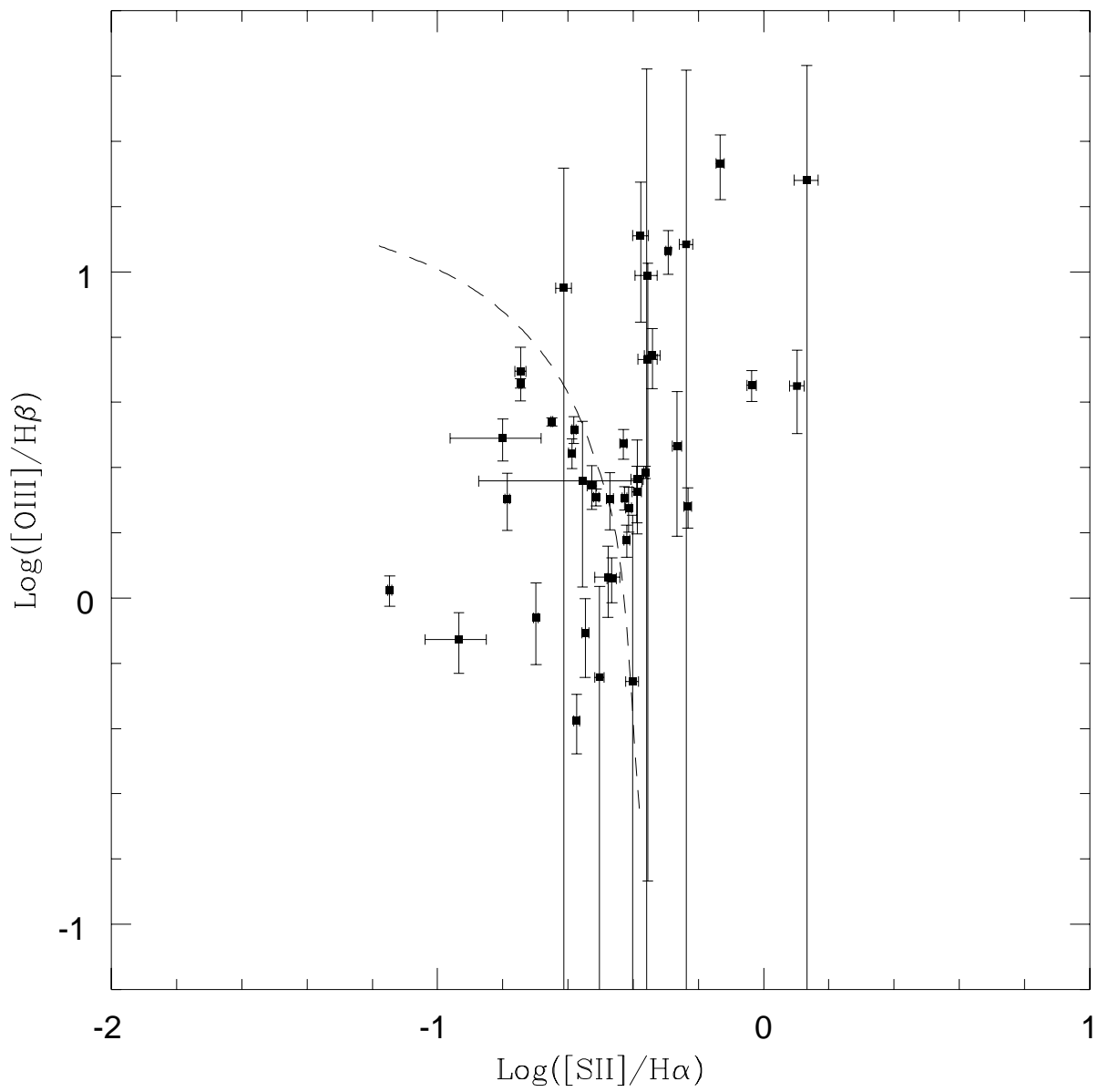


Figure 2(b)

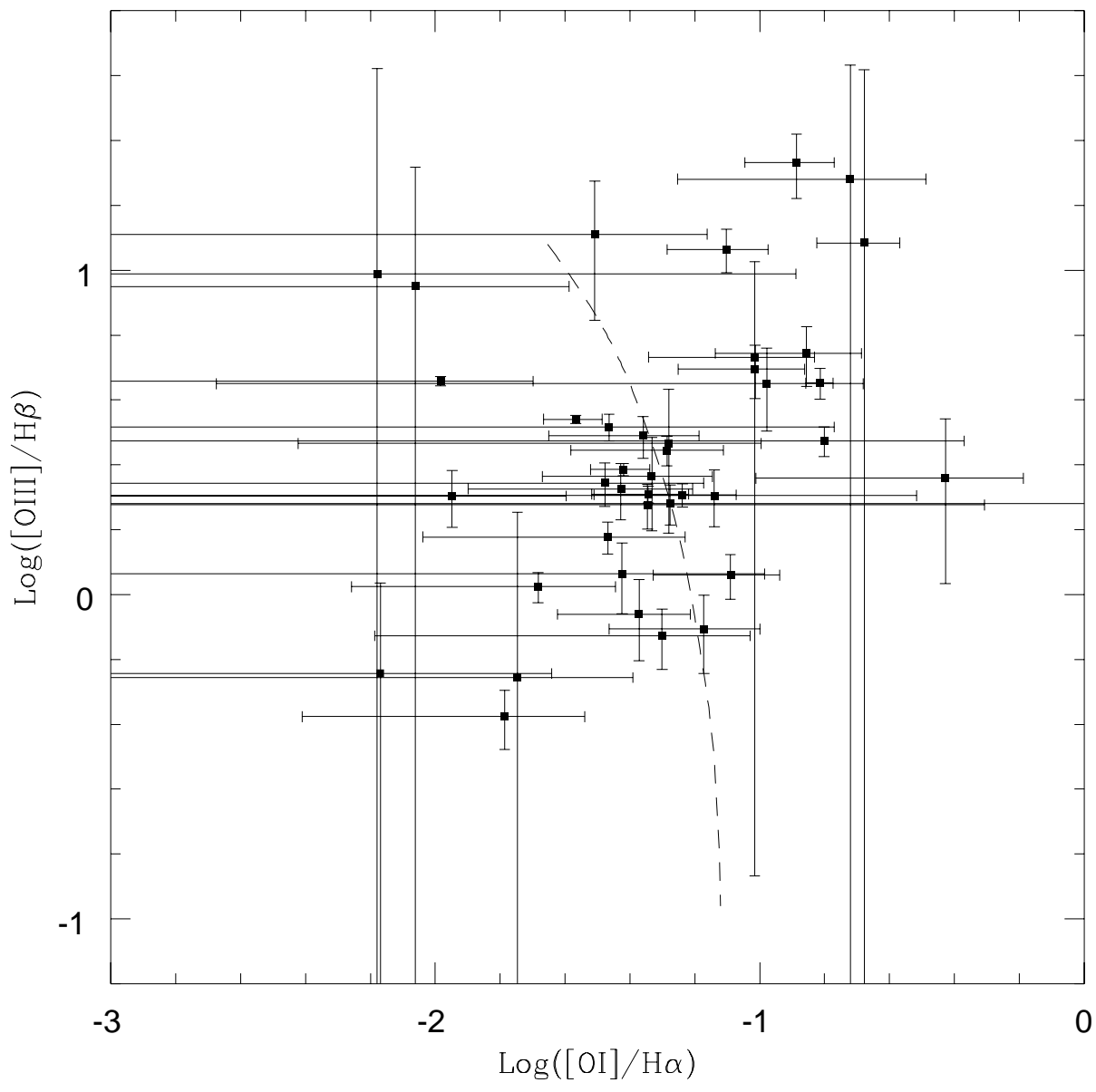


Figure 2(c)

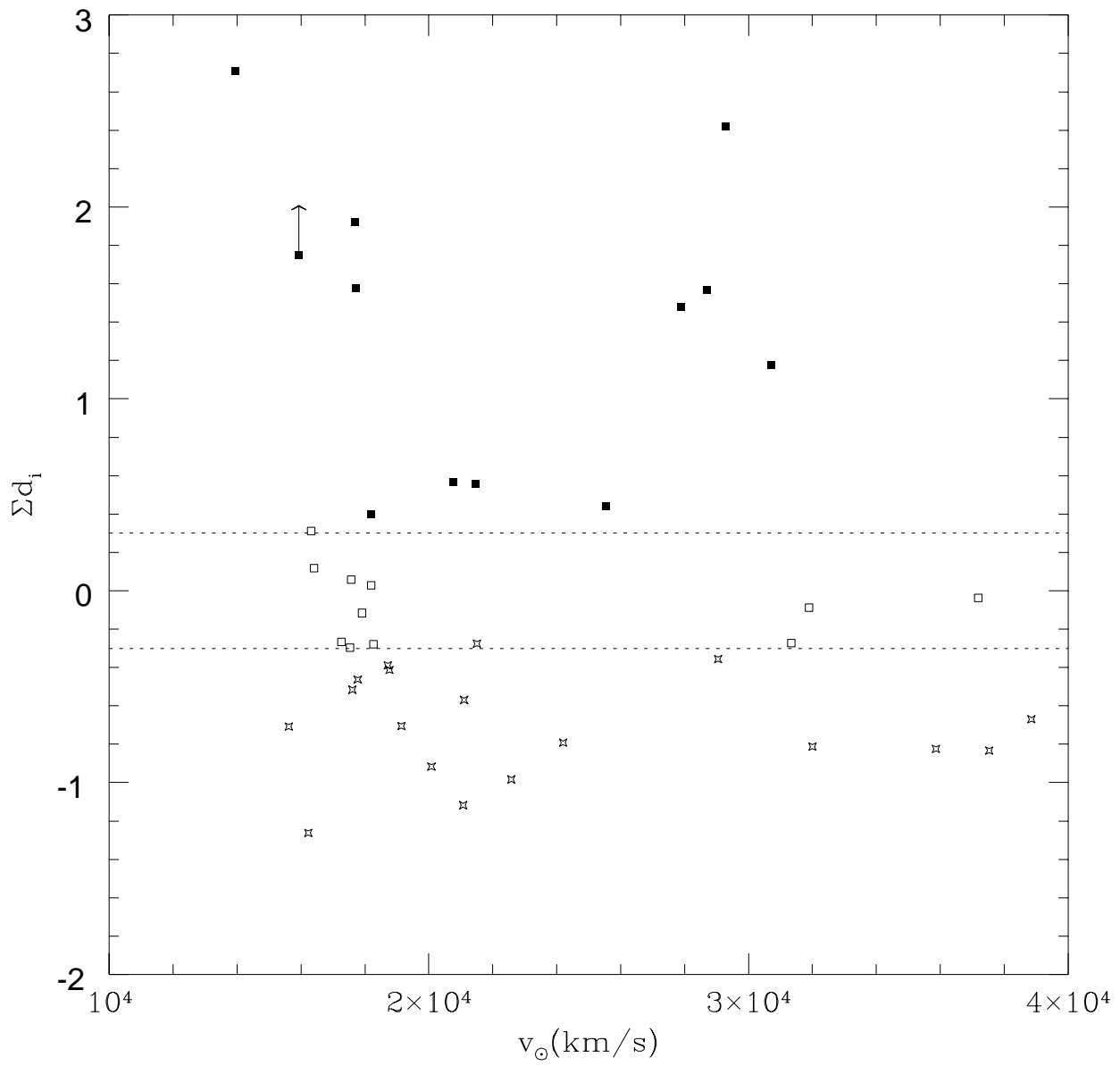


Figure 3